Table 1 Candidate measurement technologies

Technologies	Applications
Application ready	
Fiberoptic deflectometer	12
Brushless torque/stressmeter	11
Optical surface temperature sensor	10
Ultrasonic triducer	5
Isotope wear detector	3
Nonintrusive speed sensor	3
Optical absorption leak detector	1
Need development	
Spectrometry	8
Ultrasonic tomography	4
Optical densitometer	3
Raman H_2 leak detector	3
Nonintrusive hot-gas temperature sensor	2
Hydrogen leak sensor	1
Need further research	
Optical gas diagnostics	17
Gas anemometer	5
Exoelectron fatigue detector	3
Acousto-optic flaw detector	3

hypersonic engines. This article is meant as a means for the reader to only be appraised of new instrumentation technologies that may be of benefit to their control applications.

Discussion

For the sake of brevity, where two or more sensor technologies perform similar measurements and the maturity level is the same, the sensors have been grouped together under a more general name. These include technologies such as the fiberoptic pyrometer and the thermally assisted laser-induced fluorescence temperature sensor, which are listed together as optical surface temperature sensors. Emission spectrometry, such as plume emission and absorption spectrometry, including the Fabry–Perot and other laser-based spectrometers, are listed together under spectrometry. Optical gas diagnostics covers several of the two-dimensional gas temperature, pressure, density, and flow measurement technologies such as planar laser-induced fluorescence, Raman spectroscopy, coherent anti-Stokes Raman spectroscopy, laser-induced breakdown spectroscopy, and emission tomography. Hydrogen leak sensor refers to three single-point measurement technologies, using the resonant frequency shift or changes in surface acoustic waves in a hydrogen-absorbing palladium block or using a temperature sensor to measure the oxidation rate of hydrogen in a hydrogen-oxidizing platinum catalyst.

Although the nonintrusive hot-gas temperature sensor and the nonintrusive speed sensor do not necessarily provide any new measurements for the new control system concepts, they do provide nonintrusive measurements of very critical control parameters that otherwise might not have been considered as practical. For this reason, they were deemed appropriate for the accepted measurement technology list.

Each of these measurement technologies, with only four exceptions, crossfeeds from its original application in a specific propulsion system into applications in the other two types of propulsion systems. The first exceptions are the hydrogen leak sensors (three types) that do not apply to jet engines that use only hydrocarbon fuels. Optical absorption leak detection, a rocket-engine technology, also has no new control concept applications for jet engines. Lastly, the three optical desensitometers, hypersonic-engine technologies, have no new control concept applications for rocket engines. The remaining 22 technologies, however, have new control concept applications for all three types of engines.

Thirty advanced instrumentation technologies that are represented by the 17 listed measurements are recommended for consideration for appropriate developmental efforts. These technologies will enable implementation of the next-generation jet-, rocket-, and hypersonic-engine control systems.

For the inquisitive reader who would like to learn more about these technologies, a directory of measurement technologies and the references are included in the original paper.[1]

Conclusions

The primary contribution of this Note is in providing the reader with a database of the advanced instrumentation technologies targeted for advanced aerospace-propulsion control systems and in cross matching the available technologies from each type of engine to the control needs and applications of the other two types of engines.

Reference

[1]Barkhoudarian, S., Cross, G., and Lorenzo, C., "Advanced Instrumentation for Next-Generation Aerospace Propulsion Control Systems," AIAA Paper 93-2079, June 1993.

Experimental Flow Visualization for a Large-Scale Ram Accelerator

David L. Kruczynski,* Federico Liberatore,† and Michael J. Nusca‡
U.S. Army Research Laboratory, Aberdeen Proving Ground, Maryland 21005

Introduction

EXPERIMENTAL testing and gasdynamic modeling of the ram acceleration technique for in-bore projectile propulsion are being investigated at the U.S. Army Research Laboratory (ARL) under the Hybrid Inbore Ram (HIRAM) propulsion program.[1-4] This research program seeks to provide an efficient method of achieving hypervelocity (≥3 km/s) projectile gun-launch for use in high-speed impact testing applications. The ARL ram accelerator system uses a 120-mm (bore diameter) tube that is modeled after the 38-mm system at the University of Washington[5] where the technology was first demonstrated. Ram acceleration technology has also been successfully demonstrated at the Institute of St. Louis (ISL) in France.[6,7] In the ram accelerator system a projectile and obturator are injected at supersonic velocity into a stationary tube filled with a pressurized mixture of hydrocarbon, oxidizer, and inert gases. Flow stagnation on the obturator initiates combustion of the mixture, before it is discarded. A system of shock waves on the projectile, in conjunction with viscous heating, sustains combustion. The resulting energy release, which travels with the projectile, also generates high pressures that impart thrust to the projectile. The ARL experimental effort is reviewed in this Note, whereas the modeling effort is reviewed in a companion article. A great deal of synergism exists between the experimental and computational efforts in terms of validation and analysis.

Received April 12, 1995; accepted for publication April 15, 1995.

*Mechanical Engineer, Weapons Technology Directorate. Member AIAA.

†Aerospace Engineer, Weapons Technology Directorate. Member AIAA.

‡Aerospace Engineer, Weapons Technology Directorate. Senior Member AIAA.

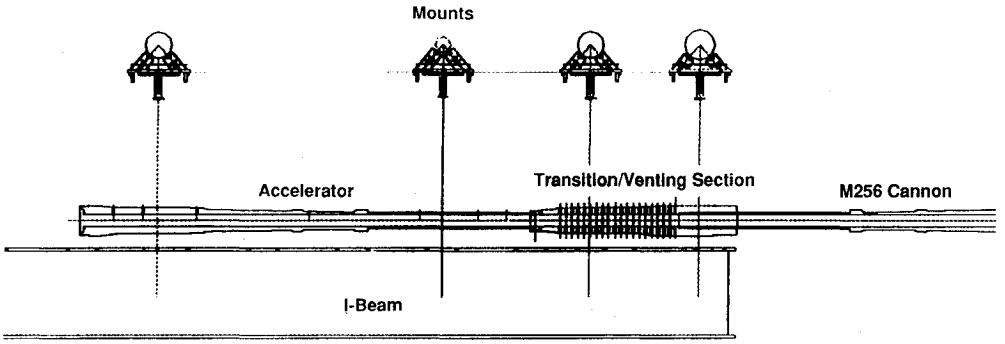

Fig. 1 ARL 120-mm ram accelerator facility. The facility consists of (from right to left) a 5.3-m-long, 120-mm bore diameter preaccelerator cannon; 2.1-m vent section; and two 4.7-m accelerator tubes (one shown).

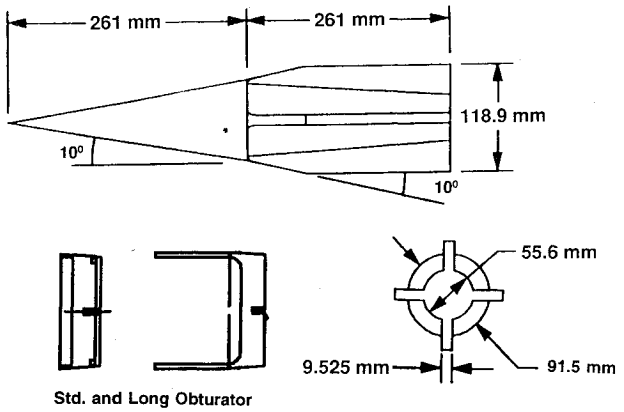

Fig. 2 Projectile and obturators.

An experimental technique to photograph transient combustion phenomena in the ram accelerator using sacrificial transparent acrylic chambers has been demonstrated. This technique allows the normal operating environment of the ram accelerator to be closely approximated. Using this technique, details of the environment during the transient starting phase, as the projectile enters the accelerator and the obturator separates, have been photographed for the first time. Steady combustion around the projectile after the obturator has been discarded has also been captured. These flow visualizations are useful in validating computational fluid dynamics (CFD) simulations as well as providing guidance concerning projectile performance.

The ARL experimental facility consists of accelerator tubes made from 120-mm M256 tank guns (see Fig. 1). Transition from the conventional (solid propellant) launcher to the accelerator is made through a transition/vent section. This section decouples the launch gun movement from the accelerator (via a sliding interface) and vents combustion gases from the conventional charge. The facility was designed to accommodate five 4.7-m accelerator tubes for a total length of 23.5 m. Current experiments utilize three accelerator tubes.[2] Gases are supplied from bottles using a compressor capable of pressurizing the tube up to 35 MPa (5100 psi). Ends of the accelerator tubes are sealed with poly vinyl chloride (PVC) diaphragms. A vacuum pump is used to evacuate the launch and vent sections. Instrumentation within the accelerator tube includes wall-mounted quartz pressure transducers. High-speed movie and still (smear) cameras are employed at the accelerator exit. Doppler radar (aimed down the tube length) is used to measure projectile velocity in-bore and at exit. A 1.8-m long, expendable, clear tube section is added to photograph the process in-bore.[1,2]

The projectile is made of high-strength aluminum alloy (4.29 kg) and consists of an axisymmetric cone-boattail body with stabilizing fins for centering in the tube (see Fig. 2). The gap between the projectile surface at maximum diameter and the tube wall is 14 mm. The accelerator tube is filled with a gas mixture of hydrocarbon fuel (CH_4), oxidizer (O_2), and diluents (e.g., N_2 and CO_2) at a pressure of 50–100 atm. Ignition of the gas is achieved by flow stagnation on the projectile obturator (0.514-kg circular disk), initially mated to the projectile in the launch gun tube (Fig. 2), then gasdynamically discarded in the accelerator tube. When the injection velocity of the projectile is greater than the sound speed of the gas a system of oblique shock waves develops on the projectile which, together with viscous heating, act to sustain combustion. This energy release travels with the projectile and thrust is generated by the action of high-pressure reacting gases on the rear part of the projectile. The gas pressure, fuel/oxidizer composition, and sound speed can be selected to achieve the desired acceleration and projectile velocity at tube exit. Diluents are used to tailor the acoustic speed of the mixture to prevent flow choking and tailor the ignition delay such that combustion takes place on the projectile afterbody.

Ram Accelerator Operation

For mixture ignition and flow starting (i.e., continuous mass flow around the projectile) the ram acceleration process currently requires the projectile be injected into the fuel/oxidizer/diluent mixture (or simply fuel) at a velocity well above the sound speed of the mixture in order to properly "swallow" and ignite the high-speed flow. In this starting regime the physics are very complex. The projectile is centered in the tube by bore-riding fins to ensure in-bore stability while allowing sufficient flow through the projectile throat (i.e., the projectile maximum diameter/tube wall clearance). This design necessitates the use of an obturator (i.e., full bore disk) behind the projectile during launch from the preaccelerator into the accelerator tube. The obturator serves to seal the preaccelerator gases behind the projectile for efficient acceleration and to prevent excessive leakage of gases in front of the projectile prior to entrance into the accelerator. Excessive buildup of gas pressure ahead of the projectile may burst the diaphragm at the accelerator entrance, before the projectile reaches it. While the obturator serves a necessary role in the preaccelerator, its function in the ram acceleration process is less clear. It has been assumed that the stagnation of flow on the obturator serves to ignite the fuel gases that once ignited remain so during acceleration of the projectile. Early experiments at the University of Washington indicated that the flow could not be ignited without the stagnation caused by the presence of an obturator.[5] However, this requirement may be strongly influenced by the geometry of the accelerator and projectile as well as the energy in the gaseous fuel and the relative Mach number of the projectile during injection. Successful experiments at the Institute of St. Louis (ISL) with a 30-mm (bore diameter) ram accelerator utilizing a railed tube (and finless projectile) and a preaccelerator that does not require an obturator (since the projectile fills the full bore

diameter) support this assumption.[7] Under some conditions the obturator can both ignite the flow and provoke an unstart. This will occur, e.g., if the obturator is too massive or if the backpressure in the preaccelerator is so high that rapid obturator separation from the projectile base is not achieved. The reacting flow may disgorge through the projectile throat area (i.e., run ahead of the projectile) causing an unstart. Avoiding this situation requires a complex and somewhat cumbersome venting arrangement that reduces the backpressure on the obturator, allowing it to separate in sufficient time to stabilize supersonic flow over the projectile. In addition the effect of perforating the diaphragm (during entrance to the accelerator) on projectile structural integrity and the starting process is largely unknown.

During testing at ARL, unstarts have occurred within the first few projectile lengths of travel in the accelerator tube. Gas chromatography indicates that some unstarts may be explained by incomplete mixing of the fuel gases, resulting in localized high-energy regions in the flow. Other unstarts are unexplained. It was believed that a better understanding of the transient starting process would assist in reducing the need for complex venting arrangements while eliminating or greatly reducing the chances for initial unstarts. Flow visualization is being used to increase the understanding of the ignition process during the critical starting phase.

Once ignition of the fuel has occurred and the obturator has separated sufficiently from the projectile base (i.e., several projectile lengths) the projectile can be said to be running with stabilized combustion, controlled by the strength of the shock system over the projectile and the energy content of the fuel. In this mode the projectile will continue to accelerate until either the energy release ahead of the projectile throat (i.e., on the forebody) exceeds that released behind the throat (i.e., on the afterbody) or the heat release behind the throat is sufficient to produce pressures that choke the flow, pushing combustion and shocks forward. The latter failure scenario corresponds to a classic unstart observed in scramjet engines. The former failure scenario is unique to ram accelerators and is attributed to the characteristics of the gaseous mixture through which the vehicle accelerates.

Projectile structural failure will also provoke an unstart. Projectile failure can be attributed to heat-induced structural weakening, unbalanced or localized pressures loads, and ablation. When an unstart occurs the projectile is often found to be destroyed. However, it has not been possible to discern if the unstart was caused by the projectile failure or if projectile failure is a result of the unstart. It was therefore necessary to develop a technique to photograph these processes with as little disturbance of the normal operating environment as possible. This effort would assist in analysis of the physical processes involved and confirm CFD simulations.

Experimental Setup for Flow Visualization

The experimental setup used in the transient visualizations is shown in Fig. 3. The primary components in the system are transparent acrylic tubes with nominal internal diameters of 120.7 mm and external diameters of 146.1 mm. The projectile maximum diameter is 119.8 mm (at the fin span). While steady combustion visualization tests at pressures in excess of 50 atm have been conducted[2] the acrylic tubes used for these studies had inconsistent mechanical properties above 20 atm. It was therefore decided to limit the fuel fill pressure to 20 atm. The first tube is nominally 0.91 m in length and is attached to the vent section and evacuated to about 0.05 atm prior to firing. This evacuated tube is attached to a flange that mates to a 1.83-m-long acrylic tube. The flange also incorporates a diaphragm that can be of any desired material. The second tube is sealed at its free end by a second diaphragm and retaining cap, which is further enclosed in a retaining box bolted to the accelerator mounting I-beam. This second tube was filled with the fuel mixture. Instrumentation employed in these studies included three 16-mm-high-speed [5–10 thousand frames per second (f/s)] color cameras focusing on various locations in the transparent tubes. A 35-mm black and white smear camera was focused near the end of the second tube to capture a still image of the projectile and obturator. In addition a standard VCR camera recorded the firings. Radars of 10 and 15 GHz were reflected down the tube length to measure projectile velocity in the tube. In addition, a scale that ran the length of the transparent tubes was used for direct measurement of projectile/obturator travel via film analysis. The fuel/oxidizer/diluent used was (on a molar basis) $2O_2 + 10N_2 + 3CH_4$ at an initial pressure of 20 atm. For this mixture the dimensionless heat release value $\Delta Q/c_pT$ (heat content over specific heat and temperature) is 3.0, sound speed is 361 m/s, and Chapman–Jouget detonation velocity is 1442 m/s. These values were obtained from Ref. 8.

To visualize established or running combustion, a 1.83-m-long acrylic tube of 127-mm i.d. and 152-mm o.d. was used. It was attached to the end of a 9.4-m-long accelerator tube (see Fig. 3). No diaphragm was used at the accelerator/acrylic tube interface to allow unimpeded transition from the standard steel accelerator tube into the transparent section. The transparent tube was sealed with an aluminum cap and PVC diaphragms, and pressurized along with the steel accelerator tube to 51 atm with the same mixture described earlier for the starting tests. The dimensionless heat release value is $\Delta Q/c_pT = 3.3$, sound speed = 361 m/s, and Chapman–Jouget

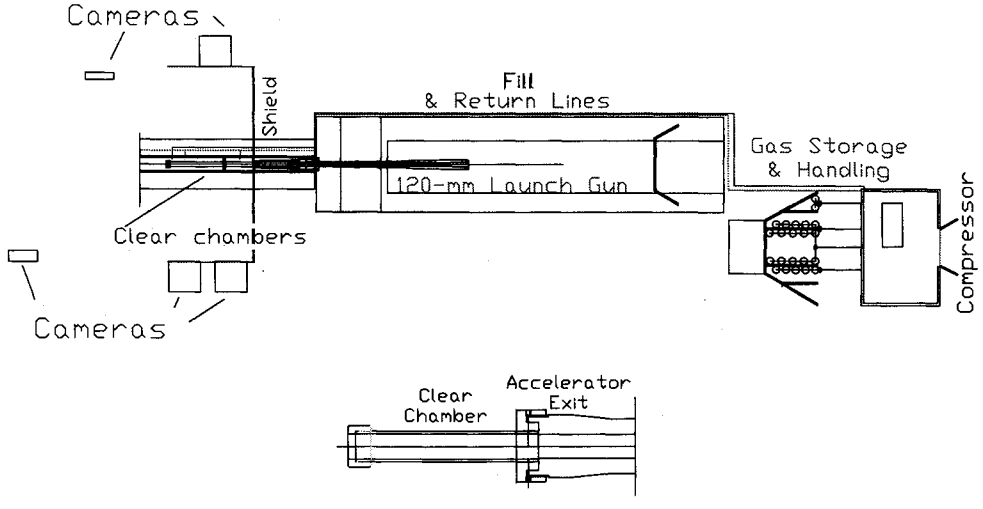

Fig. 3 Accelerator setup for clear tube starting tests (top) and running tests (bottom).

detonation velocity = 1446 m/s. This test setup is also depicted in Fig. 1.

Visualization Results

The first shot in the series (shot 30) demonstrated that the obturator does not completely seal preaccelerator gun gases from the accelerator entrance. A significant amount of light from these gases was observed ahead of the projectile in the first transparent tube. These gases preceeded the projectile by over 0.5 m, accumulated against the entrance diaphragm, and obscured observing the projectile at the entrance. The gas pressure was not sufficient to burst the diaphragm since the projectile was observed to overtake the accumulated gases during diaphragm puncture. The obturator was observed to be detached from the projectile base and tilted as the projectile entered the second transparent section. Combustion on the projectile for shot 30 initiated (as evidenced from measured tube wall pressures) and the projectile accelerated through the second chamber. However, several factors such as gas blowby, light from ignition, and the reflective aluminum projectile surface prevented clear details of the process to be observed. For the next test (shot 31) the obturator was lengthened considerably to both promote sealing and prevent tilting in the tube (see Fig. 2). In addition, the projectile surface was painted flat black with a temperature-resistant paint. Together with improved camera angles, these changes succeeded in allowing details of the combustion process to be photographed.

Shown in Fig. 4 is a series of frames from a high-speed movie camera running at 7000 f/s and aimed at a 30-deg angle towards the oncoming projectile. In the first frame of Fig. 4 the mylar diaphragm at the entrance to the second clear chamber can be seen illuminated by preaccelerator gases that have entered the evacuated test section ahead of the projectile. In the second frame the projectile nose is clearly seen piercing the diaphragm and has entered the second visualization chamber. In the third frame the projectile has entered up to approximately the midbody of the projectile. Note that no combustion in the second chamber has occurred up to this point. Images from a second movie camera (not shown) revealed that after the projectile enters the clear tube, intense combustion completely obscures it for several frames. The projectile can then be seen outrunning the intense combustion. Near the tube exit the combustion intensity begins to abate, appearing as flame structure, similar to that seen in running combustion.

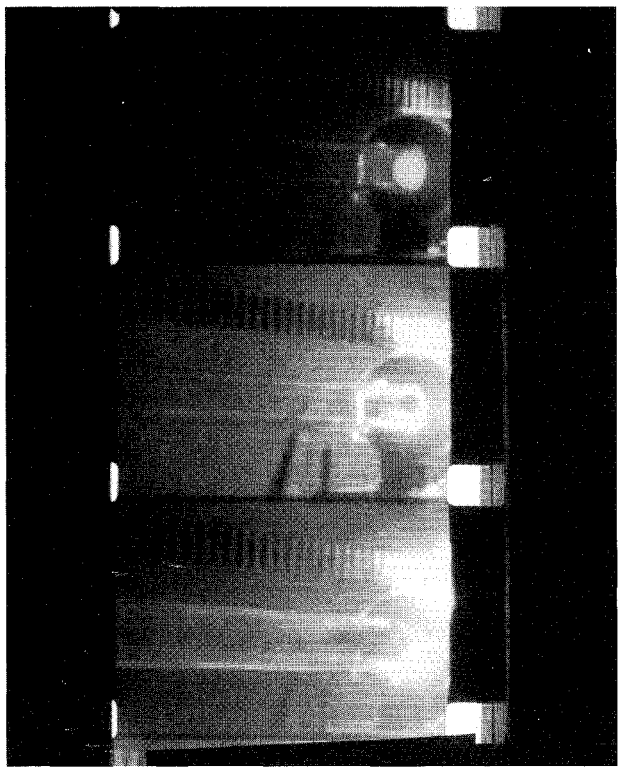

Fig. 4 Frames from high-speed movie of shot 31 (top to bottom) showing black projectile penetrating mylar diaphragm and entering second transparent tube (from the right). Note the diaphragm illuminated from behind by combustion in first tube (top frame).

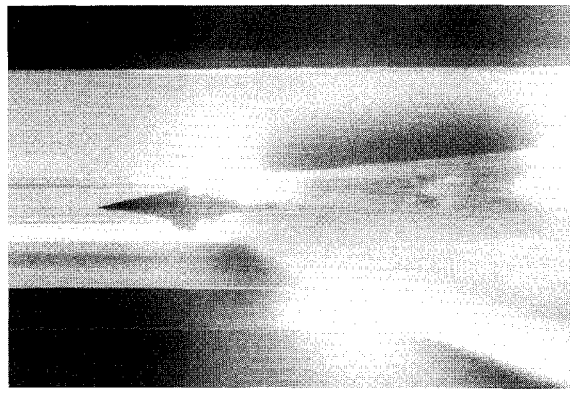

Fig. 5 Smear photograph of black projectile traveling through transparent tube (right to left) filled with combustible mixture. Note the absence of combustion on conical forebody and luminous combustion established on projectile fins and afterbody. The discarded obturator is located approximately one projectile length to the right of (behind) the projectile.

Figure 5 is a black and white smear (still) camera shot of the projectile just before exit from the combustion chamber (1.8 m of travel in combustible mixture). At this point most of the forebody is visible, while the aft end of the projectile is immersed in combustion. The obturator is seen trailing the projectile by about 360 mm or about two-thirds of a projectile length. Note that the obturator appears to be broken, allowing flow to pass through. Note also that the projectile nosetip appears to suffer little or no damage from diaphragm puncture and there is no indication of combustion in the nose region. The projectile velocity and Mach number at this point are 1300 m/s and 3.6, respectively.

Figure 6 is a side view of a projectile accelerating through a visualization section positioned at the end of the accelerator tube (see Fig. 3). The sequence of frames is from a high-speed movie running at 5000 ft/s. Since the obturator is well downstream of the projectile at this point the combustion profile through this section is relatively constant with the primary combustion zone located near the projectile midsection and the leading edges of the fins. The transparent tube used in this test is slightly oversize (127 mm) leaving 7 mm (diameter) clearance around the fins. This clearance allows the projectile to pitch in-bore. Combustion around the projectile does not appear to be greatly effected by the projectile pitch. The peak projectile velocity and Mach number in this section are 1480 m/s and 4.1, respectively.

The visualization results presented previously illustrate several interesting phenomena. As the projectile enters the optically clear combustion chamber, with the obturator closely behind, flow stagnates on the obturator surface and bulk ignition occurs in the flow extending from the obturator forward and covering about two-thirds of the projectile. This combustion is very intense as evidenced by extreme light emission. As the projectile accelerates away from the obturator the combustion moves back on the projectile body and becomes less intense. The combustion that now stabilizes near the projectile midbody also appears to develop structure. When the obturator is downstream from the projectile base (i.e., several projectile lengths) the combustion appears stabilized and located on and near the fin leading edges.

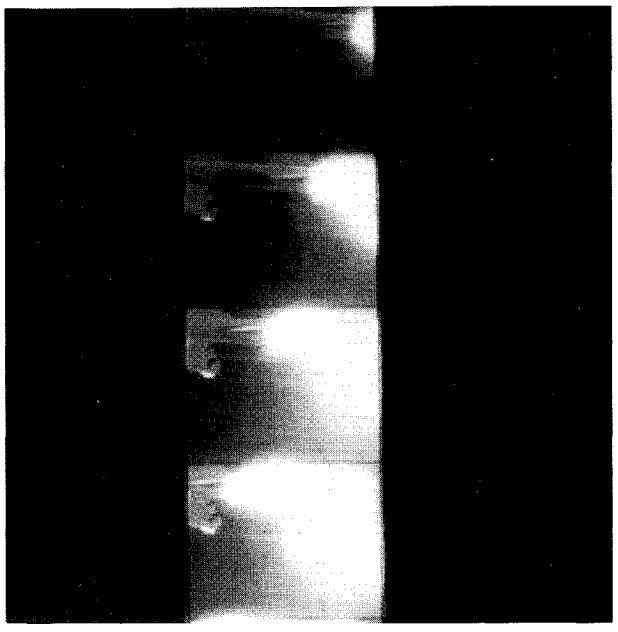

Fig. 6 Frames from a high-speed movie of shot 27 as the silver projectile accelerates through the transparent tube with luminous combustion established on the afterbody (projectile traveling right to left, frames progressing top to bottom).

Conclusions

Flow visualization techniques for transient and steady combustion in the ram accelerator have been demonstrated. Flow visualizations indicate intense combustion around the projectile until the obturator is far downstream of the projectile; stable combustion is then established on the projectile mid- and aft-sections. These observations suggest that reduction in the number of unstarts, as well as potential performance increases, may be achieved by control of the obturator location relative to the projectile during the starting process.

Acknowledgments

A. Horst, T. Minor, and D. Kooker have supported both the experimental and numerical simulation aspects for the HIRAM project since its inception and have contributed to this work through various technical discussions. C. Ruth, A. Koszoru, J. Hewitt, and J. Tuerk provided support in the experimental and photographic aspects of the project.

References

[1]Kruczynski, D. L., "Flow Visualization of Steady and Transient Combustion in a 120-mm Ram Accelerator," AIAA Paper 94-3344, June 1994.

[2]Kruczynski, D. L., "Experiments in a 120-MM Ram Accelerator Including Flow Visualization," *Proceedings of the 31st JANNAF Combustion Subcommittee Meeting*, Vol. 1, CPIA Pub. 620, 1994, pp. 102–110.

[3]Nusca, M. J., "Reacting Flow Simulation for a Large Scale Ram Accelerator," AIAA Paper 94-2963, June 1994.

[4]Nusca, M. J., "Numerical Simulation of Ram Accelerator Performance Including Transient Effects During Initiation of Combustion and Sensitivity Studies," *Proceedings of the 31st JANNAF Combustion Subcommittee Meeting*, Vol. 1, CPIA Pub. 620, 1994, pp. 111–118.

[5]Hertzberg, A., Bruckner, A. P., and Bogdanoff, D. W., "Ram Accelerator: A New Chemical Method for Accelerating Projectiles to Ultrahigh Velocities," *AIAA Journal*, Vol. 26, No. 2, 1988, pp. 195–203.

[6]Giraud, M., Legendre, J.-F., and Simon, G., "Ram Acceleration at ISL; First Experiments in 90 mm Caliber," *Proceedings of the 42nd Meeting of the Aeroballistic Range Association*, Adelaide, Australia, 1991, pp. 12–16.

[7]Smeets, G., Seiler, F., Patz, G., and Srulijes, J., "First Results Obtained in a 30 mm Caliber Scram Accelerator Using a Rail Tube for Cylindrical Projectiles," *Proceedings of the 25th International Symposium on Combustion* (Irvine, CA), Combustion Inst., Pittsburgh, PA, 1994, pp. 21–35.

[8]Liberatore, F., "Ram Accelerator Performance Calculations Using a Modified Version of the NASA CET89 Equilibrium Chemistry Code," U.S. Army Research Lab. ARL-TR-647, Aberdeen Proving Ground, MD, Dec. 1994.

Study on Thermal Strain Using Subscale Specimens

F. H. Su,* S. W. Wang,* and H. C. Perng†
Chung Shan Institute of Science and Technology, Lung-tan 32526, Taiwan, Republic of China

Introduction

A NONLINEAR relationship between hoop strains and temperatures is often observed in strain evaluation cylinder (SEC) experiments. This phenomenon is not consistent with the simplified equation mentioned in a conventional manual[1] and recently applied in round-robin analysis[2] for assessing stress-free temperature and thermal expansion coefficient of propellant. Moreover, the traditional measure techniques, x-ray and intermicrometer, have some drawbacks from the experimental point of view.

This work elucidates a modified equation-resolving experimental disagreement with the simplified equation, describes a technique improving drawbacks of measurement, and discusses finite element analysis (FEA) results pointing to displacement rather than strain for comparison between analysis and the SEC experiment in the geometric nonlinear case.

Theory Consideration

Linear Solution

According to the ICRPG manual,[1] a simplified solution for SEC data analysis is defined as follows:

$$\varepsilon = -(p/2)(\lambda^2 - 1)(\beta T + l) \tag{1}$$

in which ε, p, λ, β, T, and l are, respectively, the hoop strain, Parr factor, grain's external diameter/mandrel diameter, volume thermal expansion coefficient, temperature, and constant. Equation (1) shows that the relationship between hoop strains and temperatures is linear, which is not consistent with the report depicting a nonlinear phenomena.[2] Having considered the deformed configuration of propellant grain, a modified solution can be derived as follows:

$$\varepsilon = -(p/2)\{[dm/d(T)]^2\lambda^2 - 1\}(\beta T + l) \tag{2}$$

in which dm is the mandrel diameter and $d(T)$ is the inner-bore diameter of propellant grain at different temperatures. Thus, Eq. (2) indicates a nonlinear relationship of hoop strains vs temperatures and leads to a convex shape which is consistent with the data of the report.[2]

Received Dec. 31, 1993; revision received Oct. 14, 1994; accepted for publication May 16, 1995.

*Assistant Scientist, Fourth Division.
†Senior Scientist, Fourth Division. Member AIAA.